NGL-05-002-007

COSMIC-RAY NEGATRON AND POSITRON SPECTRA OBSERVED NEAR FORT CHURCHILL IN 1968

K. P. Beuermann, C. J. Rice,
E. C. Stone, and R. E. Vogt

CALIFORNIA INSTITUTE OF TECHNOLOGY

PASADENA, CALIFORNIA

NGL-05-002-007

COSMIC-RAY NEGATRON AND POSITRON SPECTRA OBSERVED NEAR FORT CHURCHILL IN 1968

K. P. Beuermann, C. J. Rice,
E. C. Stone, and R. E. Vogt

California Institute of Technology
Pasadena, California, 91109, U.S.A.

August 1969
SRL-69-7

COSMIC-RAY NEGATRON AND POSITRON SPECTRA OBSERVED NEAR FORT CHURCHILL IN 1968*

K. P. Beuermann+, C. J. Rice,
E. C. Stone, and R. E. Vogt

California Institute of Technology
Pasadena, California, 91109, U.S.A.

SUMMARY

The differential energy spectra of cosmic-ray positrons and negatrons between 12 and 210 MeV have been measured with a balloon-borne magnetic spectrometer launched from Fort Churchill, Canada, in summer 1968. Since the geomagnetic cutoff varies with time, separate spectra for the local day and night intervals are presented. In addition, the corrections for atmospheric secondary electrons are discussed in detail. The solar modulation of the positron flux is compared with the modulation of cosmic-ray nuclei.

An understanding of the origin of the cosmic-ray electron component and its modulation in the solar system requires accurate measurements of the shape and charge composition of the primary electron spectrum at the Earth. At present, information on the long-term variations of the primary cosmic-ray

*Work supported by the National Aeronautics and Space Administration under Grant Number NGL 05-002-007.

+Present address: University of Kiel, Kiel, Germany.

electron flux (positrons plus negatrons) is inconclusive [1-5] and has not yet led to a consistent picture of the relative solar modulation of electrons. The absolute solar modulation of positrons can be determined by comparing the spectrum measured near the Earth with the equilibrium spectrum calculated for positrons originating in cosmic-ray interactions in interstellar space. The modulation thus derived will be valid provided that this process is the only significant source of positrons and that the physical data used in the calculations are correct. We have reported initial results on positron modulation between 12 and 220 MeV elsewhere [6], and results for higher energies have been reported by Fanselow et al. [7].

In this paper we present improved data and extend our earlier discussion of the energy spectrum and charge composition of primary cosmic-ray electrons between 12 and 210 MeV. Our measurements were made with a balloon-borne magnetic spectrometer. The data have been derived from three flights launched from Fort Churchill, Canada, on 15 July, 20 July, and 28 July 1968. A schematic cross section of the detector system is shown in Figure 1. The particle trajectory is determined by two wire spark chambers of four gaps each with magnetostrictive readout. A triple coincidence of the two plastic scintillator telescope counters and the Lucite Čerenkov counter initiates the analysis of an event. A magnet guard counter in active anticoincidence excludes particles whose trajectories intersect the pole faces of the magnet. The geometry factor of the system is 3.7cm^{2}sr between 200 and 25 MV and then decreases gradually to 1.5cm^{2}sr

at 6 MV. Momentum resolution is constant at 25% FWHM below 100 MV and increases to 50% at 200 MV.

The determination of extraterrestrial electron fluxes with a balloon-borne detector is complicated by the geomagnetic field and by the residual layer of atmosphere above the instrument. These effects are especially significant at electron energies below several hundred MeV. We gave particular attention therefore to the corrections for atmospheric secondary electrons and to the consideration of the diurnal geomagnetic cutoff variations occurring near Fort Churchill. (For a recent discussion of the diurnal intensity variations near Fort Churchill see Ref. [8].) All flights were launched in the early evening in order that the instrument would rise through the 100 g/cm^2 atmospheric level after onset of the local geomagnetic nighttime interval. We thus obtained intensity versus altitude data which could be used to correct the nighttime fluxes for atmospheric secondaries. Each flight continued well into the following day and showed a pronounced increase of the electron flux below about 100 MeV during the morning transition. The differential energy spectra of negatrons and positrons measured at the detector during the local day and night intervals are shown in Figure 2. The daytime spectra, when corrected for the contribution of atmospheric secondaries, exhibit a charge ratio nearly equal to unity over the full energy range of our measurements. Such a ratio is expected for splash and re-entrant albedo electrons of mixed origin from $\Pi \rightarrow \mu \rightarrow e$ decay and from electromagnetic cascades. Our results therefore support the interpretation of the daytime

flux as predominantly re-entrant albedo electrons. During the nighttime interval the lower geomagnetic cutoff excludes re-entrant albedo while allowing primary cosmic-ray electrons to reach the Earth. The strong day-night intensity difference in our lowest energy interval indicates that the nighttime geomagnetic cutoff was below our analysis threshold, which corresponds to 11.8 MV at the top of the atmosphere.

At our float depth of 2.4 g/cm^2 the measured flux contains a significant component of secondary electrons produced in the residual atmosphere above the detector. Our method for the separation of the atmospheric secondary component from the locally observed flux is based upon the measurement of intensity as a function of atmospheric depth and upon a detailed knowledge of the theoretical depth dependence of the secondary flux. The propagation of the secondary electron component through the atmosphere can be described by a set of transport equations for negatrons, positrons, and photons. These equations have been solved numerically by one of us [9]. The calculations yield the shape of the growth curves for the different particle species. In general the secondary flux does not grow linearly with depth, contrary to the assumption which is commonly made. The depth dependence of the residual primary positrons and negatrons can be similarly calculated given an incident spectrum.

Using our measured intensity as a function of atmospheric depth, we make a least squares fit of a linear combination of two curves, one having the functional depth dependence of the calculated atmospheric secondaries and the other that of the

residual primaries. The best fit determines the contribution of each component. Separate fits are made for negatrons, positrons, and total electrons in each of 5 energy intervals; seven data points between 2.4 and 42 g/cm^2 are used for each fit. An iterative procedure is used since the depth dependence of the residual primary flux depends upon the unknown primary spectrum at the top of the atmosphere. In Figure 3 we show as examples the measured growth curves (raw data points) of positrons and negatrons for three selected energy intervals and the fitted residual primary and atmospheric secondary contributions. The χ^2 probability P for each fit is indicated in the figure. In the 6.5-12.5 MeV interval (measured at the detector) the existence of a primary component for both negatrons and positrons is clearly evident. For the 50-100 MeV interval the measured growth curves agree with the theoretical growth of secondaries within the statistical errors and the fitting results in a small negative flux of primaries. Therefore, in this energy interval, we can derive only an upper limit for the primary flux. In the 100 to 200 MeV interval we deduce a finite primary flux. Our data therefore suggest a dip in the primary spectrum at $\sim$ 70 MeV.

In Figure 4 we show the raw spectra of positrons and negatrons observed at an atmospheric depth of 2.4 g/cm^2 together with their separation into primary and secondary components which result from the least square fitting process described above. For the 50-100 MeV interval a 1σ upper limit from zero flux is plotted.

We correct the residual primary spectra derived at a depth of 2.4 g/cm^2 for energy loss in the overlying atmosphere and for a background contribution due to photon interactions in the Lucite Čerenkov counter (the photon corrections are based upon calibrations of the instrument with γ-rays from the Caltech synchrotron). The derived differential spectrum of primary cosmic-ray electrons (positrons plus negatrons) in 1968 is shown in Figure 5a. Improved corrections have resulted in flux values and energy intervals that differ slightly from those presented earlier [6]. In addition to the results obtained by other investigators [5, 10, 11] in 1967 and 1968, we have included in Figure 5a the electron spectrum of Fanselow et al.[7] measured in 1965 and 1966 with another magnetic spectrometer. In the regions of overlap the electron spectra of Simnett and McDonald [10] and Fan et al.[11], which are derived from satellite observations outside the magnetosphere, agree well with the spectrum derived from our observations.

No significant long-term variations in the electron spectrum below about 20 MeV seem to occur [10]. Similarly, at high energies no large modulation effects are expected. The intermediate energy range between about 20 MeV and several GeV is subject to controversy. Although some of the differences among the spectra quoted by different investigators may be attributable to solar modulation, the presence of instrumental effects and the application of different corrections for atmospheric secondaries may also be responsible. For example, Rockstroh and Webber [5] have derived a modulation function for cosmic-ray electrons between 10 MeV

and 2 GeV by comparing their spectrum obtained in 1966 with our 1968 results on primary electrons below 220 MeV [6] and their own 1968 spectrum above 200 MeV. However, we note that the raw flux of electrons between 15 and 200 MeV observed by Rockstroh and Webber [5] during daytime is lower by a factor of about two than our own daytime observations (Figure 2), which were made only 11 days earlier at nearly the same atmospheric depth. Independent of whether this difference is due to a systematic difference in the response of the Caltech magnetic spectrometer and Rockstroh and Webber's lead glass spectrometer or due to an unexplained short term temporal variation, we feel that, at present, conclusions concerning the relative solar modulation are likely to suffer from the lack of internal consistency among the available electron spectra.

In Figure 5b our measured 1968 primary cosmic-ray positron fluxes are shown together with those obtained by Fanselow et al. [7] in 1965 and 1966. In an earlier paper [6], we deduced the absolute solar modulation of positrons in 1968 for energies between 12 and 220 MeV from a comparison of our measured positron spectrum with an interstellar equilibrium spectrum calculated by Ramaty and Lingenfelter [12] for positrons originating in cosmic-ray collisions with interstellar matter. (Curve e_S^+ in Figure 5b) The calculated spectrum agrees reasonably well with the measured fluxes at the higher energies where essentially no solar modulation is expected. This agreement lends confidence to the assumption that the calculated spectrum is a fair representation of the local interstellar positron intensity. At lower energies,

however, the interstellar flux is reduced significantly near Earth, and the modulation appears strongest at $\sim$ 70 MeV. The diffusion-convection theory of solar modulation in a simple form predicts a modulation function

$$F(R) = \exp\left[-\eta/\beta\, f(R)\right]$$

where R is the rigidity, βc is the particle velocity, and η is a rigidity independent parameter characteristic of the state of the interplanetary medium. In our earlier paper [6] we suggested on the basis of our measured positron spectrum that

$$\begin{aligned} f(R) &= R \quad \text{for} \quad R > R_o = 70\ \text{MV} \\ f(R) &= R_o^2/R \quad \text{for} \quad R < R_o = 70\ \text{MV} \end{aligned} \tag{1}$$

and the parameter $\eta = 0.5$. We discussed the consequences of this model, which makes explicit the decreasing modulation at low rigidities implied by our data. Although it is a good fit to our data, it is not the only possible fit.

Nucleonic data indicate that

$$\begin{aligned} f(R) &= R^{\delta} \quad \text{for } R > R_o \\ f(R) &= R_o \quad \text{for } R < R_o \end{aligned} \tag{2}$$

with $\delta \approx 0.5 - 1$ and $R_o \approx 0.3 - 1$ GV. Using this functional form, Fanselow et al. [7] have made a fit to their positron data above 173 MV with $\delta \simeq 1$, $R_o = 0.3$ GV, and $\eta = 0.6$ GV. The modulated spectrum derived from the interstellar spectrum with these values is shown as curve (a) in Figure 5b. While adequate at energies above 200 MeV, this set of parameters is unsatisfactory

(χ^2 probability $P << 0.01$) for the lower energies covered by our measurement. A better fit to our data is obtained with an R_o = 175 MV, shown as curve (b) in Figure 5b ($P = 0.28$). This model implies a strong modulation below 20 MV in contrast to the decreasing modulation given by Equation (1). Simnett and McDonald [10] have pointed out that their measured electron spectrum between 2 and 20 MeV is compatible with a sole origin in the galactic knock-on component if solar modulation is insignificant at these energies. Since our data clearly indicate a strong modulation near 100 MeV, only a decreasing modulation at lower energies, as exemplified by Equation (1) would be consistent with the knock-on hypothesis. However, the statistical accuracy of our data does not allow us to dismiss solar modulation as described by Equation (2). Both models adequately describe the pronounced modulation evident in the region near 100 MeV.

REFERENCES

1. W. R. Webber, J. Geophys. Res., 72, 5949, 1967.
2. J. L'Heureux, P. Meyer, S. D. Verma, and R. Vogt, Can. J. Phys., 46, S 896, 1968.
3. J. A. M. Bleeker, J. J. Burger, A. J. M. Deerenberg, A. Scheepmaker, B. N. Swanenburg, and Y. Tanaka, Can. J. Phys., 46, S 911, 1968.
4. J. A. M. Bleeker, J. J. Burger, A. J. M. Deerenberg, A. Scheepmaker, B. N. Swanenburg, and Y. Tanaka, Phys. Rev. Letters, 22, 1325, 1969.
5. J. Rockstroh and W. R. Webber, University of Minnesota Preprint No. CR-126.
6. K. P. Beuermann, C. J. Rice, E. C. Stone, and R. E. Vogt, Phys. Rev. Letters, 22, 412, 1969.
7. J. L. Fanselow, R. C. Hartmann, R. H. Hildebrand, and Peter Meyer, The University of Chicago, Preprint No. EFI 69-22.
8. M. H. Israel and R. E. Vogt, J. Geophys. Res., 74, Sept. 1969 (to be published).
9. K. Beuermann, to be published.
10. G. M. Simnett and F. B. McDonald, Goddard Space Flight Center Preprint No. X-611-68-450.
11. C. Y. Fan, J. L'Heureux, and P. Meyer, private communication.
12. R. Ramaty and R. E. Lingenfelter, Phys. Rev. Letters, 20, 120, 1968.

FIGURE CAPTIONS

Fig. 1 Schematic cross section of the detector system.

Fig. 2 Differential energy spectra of the raw flux of positrons and negatrons measured in July 1968 during the nighttime interval at 2.4 g/cm^2 and during the daytime interval at 2.3 g/cm^2 atmospheric depth.

Fig. 3 Differential flux vs. atmospheric depth for negatrons and positrons in three energy intervals. The primary and secondary components are derived by the least squares fitting technique described in the text. The total flux is the sum of the primary and secondary flux.

Fig. 4 Differential energy spectra of positrons and negatrons measured at 2.4 g/cm^2 during nighttime (raw flux). Also shown is the separation into primary and secondary components derived from the growth curves. Error bars represent statistical errors obtained from the least squares fit.

Fig. 5 (a) Differential kinetic energy spectra of extra-terrestrial cosmic-ray electrons. The year of the measurement is indicated in front of the references. (b) Differential kinetic energy spectra of extra-terrestrial cosmic-ray positrons. The solid curve (e_S^+) is the interstellar positron spectrum calculated for the collision source with an integral pathlength

of 4 g/cm^2 (see Ref. 12). The modulated curves a and b are described in the text. Error bars of the present work represent statistical plus estimated systematic error limits.

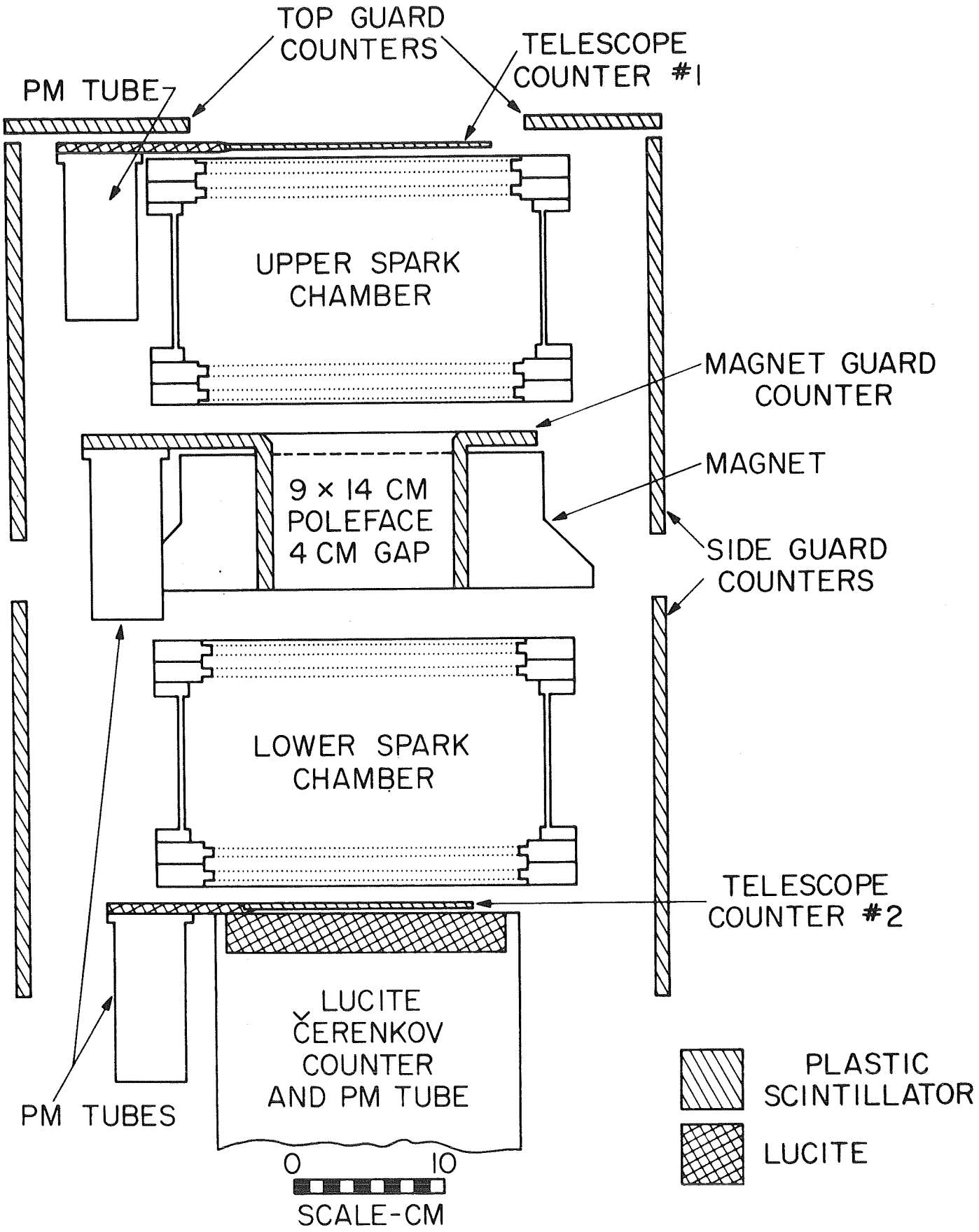
TOP GUARD COUNTERS
TELESCOPE COUNTER #1
PM TUBE
UPPER SPARK CHAMBER
MAGNET GUARD COUNTER
MAGNET
9 × 14 CM POLEFACE 4 CM GAP
SIDE GUARD COUNTERS
LOWER SPARK CHAMBER
TELESCOPE COUNTER #2
LUCITE ČERENKOV COUNTER AND PM TUBE
PM TUBES
PLASTIC SCINTILLATOR
LUCITE
0
10
SCALE-CM

FIGURE 1

DIFFERENTIAL FLUX (M^2·SEC·SR·MeV)$^{-1}$
POSITRONS
DAY
NIGHT
1
10^{-1}
10
100
KINETIC ENERGY (MeV)
DIFFERENTIAL FLUX (M^2·SEC·SR·MeV)$^{-1}$
NEGATRONS
DAY
NIGHT
1
10^{-1}
10
100
KINETIC ENERGY (MeV)

FIGURE 2

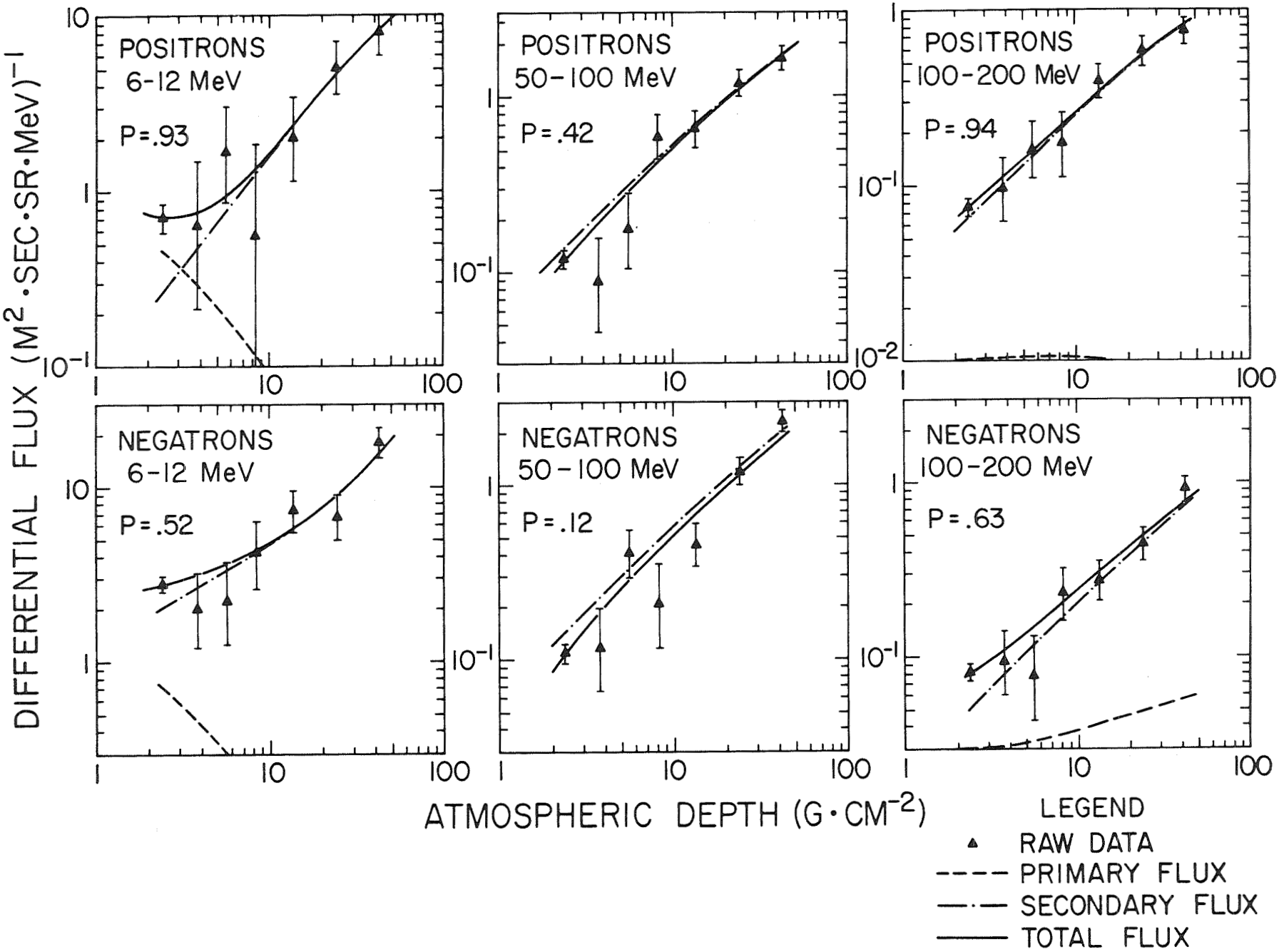
POSITRONS
6-12 MeV
P=.93
POSITRONS
50-100 MeV
P=.42
POSITRONS
100-200 MeV
P=.94
NEGATRONS
6-12 MeV
P=.52
NEGATRONS
50-100 MeV
P=.12
NEGATRONS
100-200 MeV
P=.63
DIFFERENTIAL FLUX (M^2·SEC·SR·MeV)$^{-1}$
ATMOSPHERIC DEPTH (G·CM^{-2})
LEGEND
RAW DATA
PRIMARY FLUX
SECONDARY FLUX
TOTAL FLUX

FIGURE 3

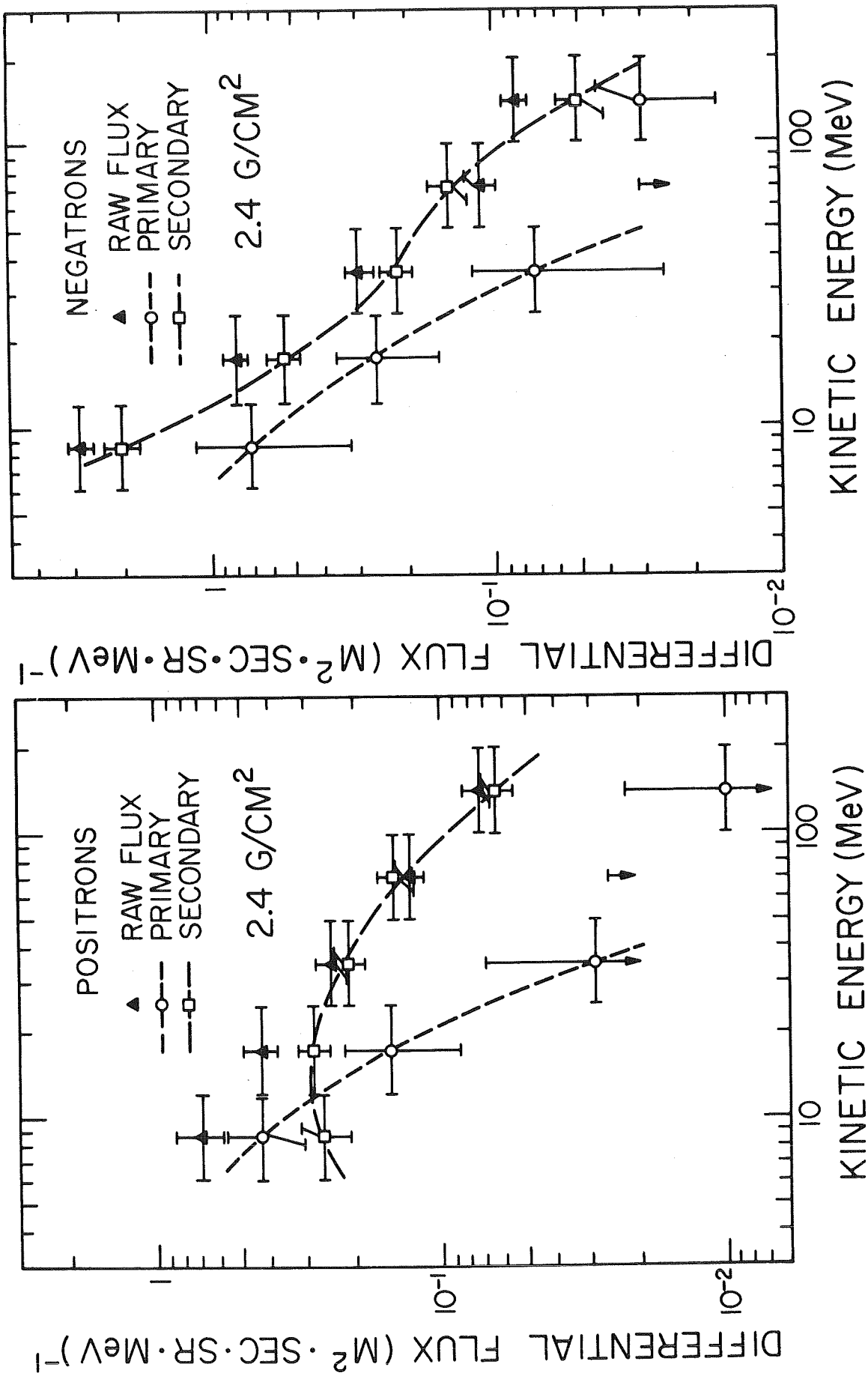
NEGATRONS
RAW FLUX
PRIMARY
SECONDARY
2.4 G/CM^2
DIFFERENTIAL FLUX (M^2·SEC·SR·MeV)$^{-1}$
KINETIC ENERGY (MeV)
POSITRONS
RAW FLUX
PRIMARY
SECONDARY
2.4 G/CM^2
DIFFERENTIAL FLUX (M^2·SEC·SR·MeV)$^{-1}$
KINETIC ENERGY (MeV)

FIGURE 4

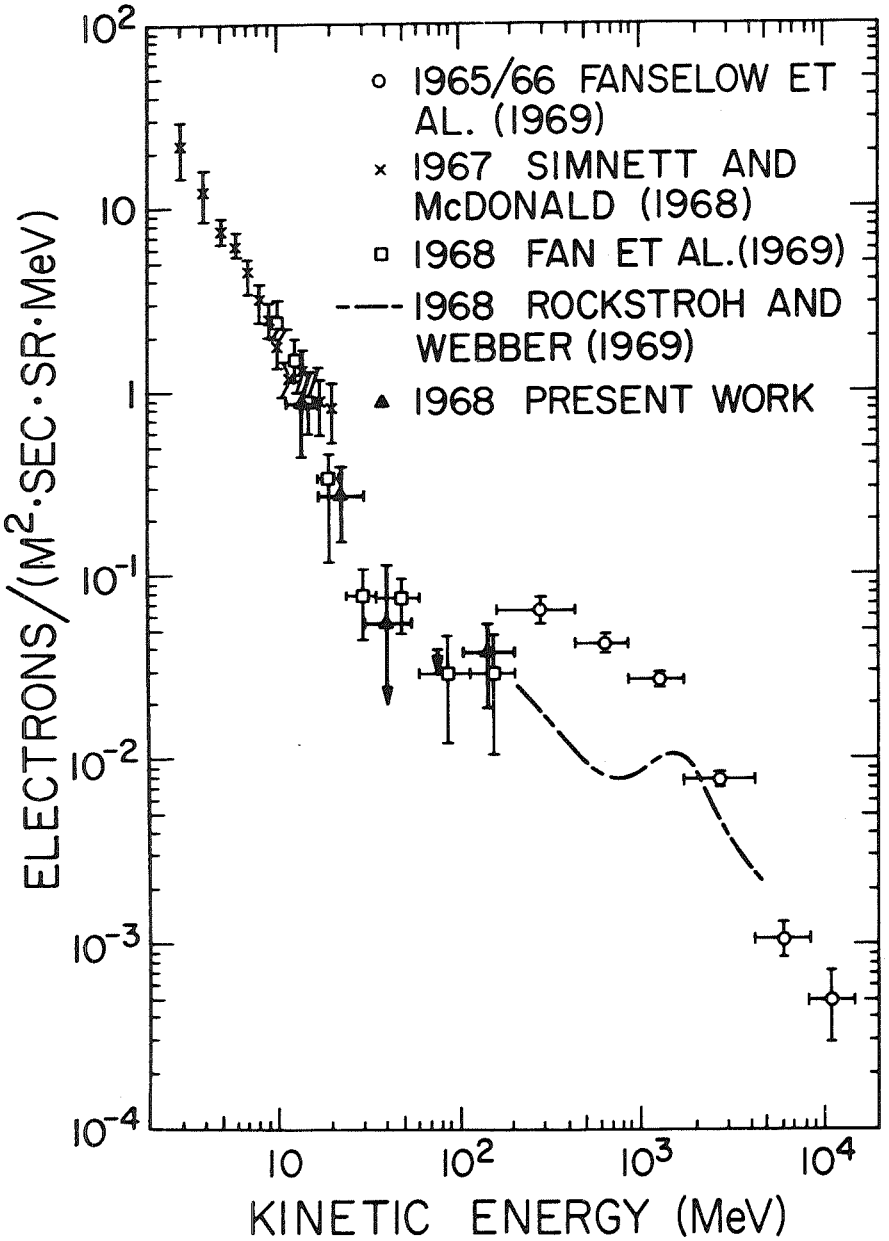

5a

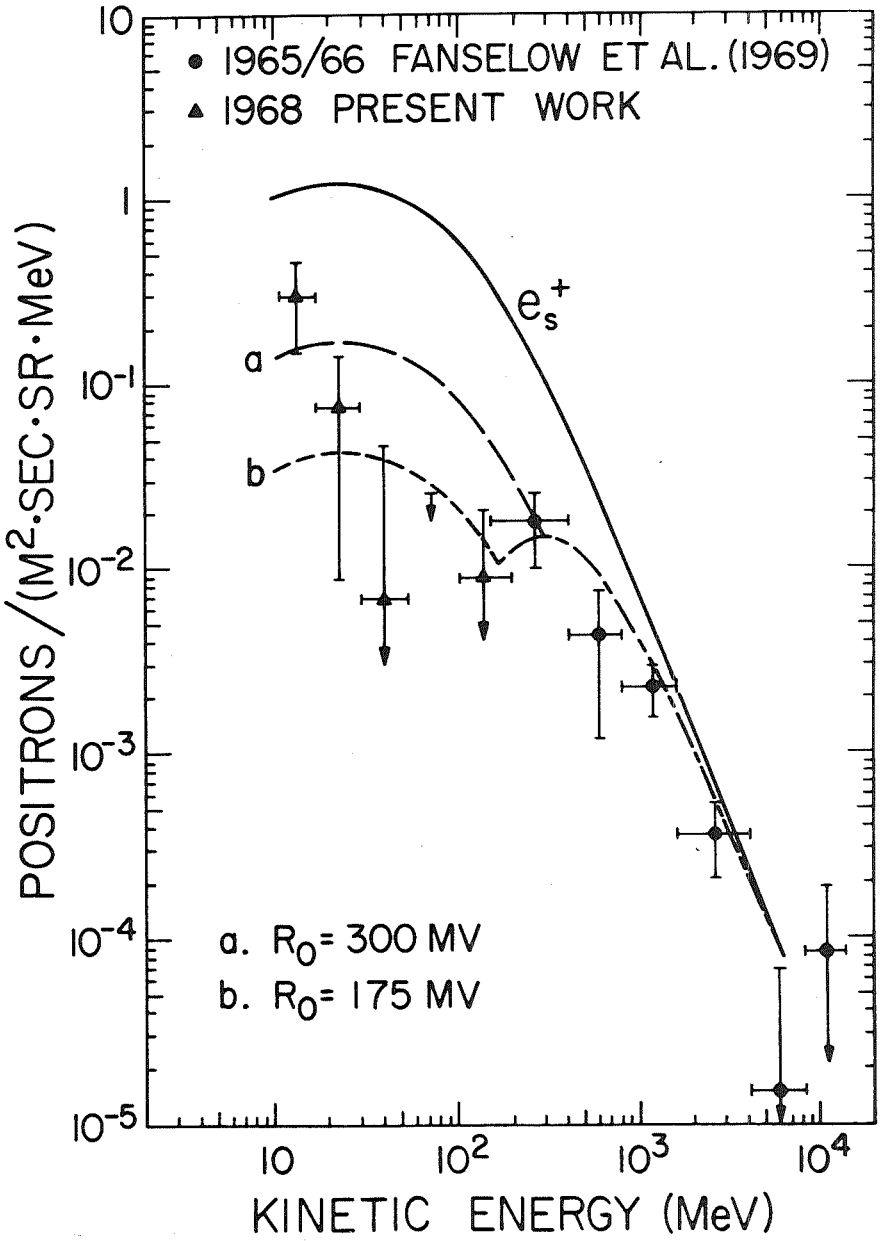

5b

FIGURE 5